Inorganic Chemistry

Article

pubs.acs.org/IC

Photoreduction of Pt(IV) Chloro Complexes: Substrate Chlorination by a Triplet Excited State

Tharushi A. Perera, Mehdi Masjedi, and Paul R. Sharp*

Department of Chemistry, University of Missouri, 125 Chemistry Building, Columbia, Missouri 65211-7600, United States

Supporting Information

ABSTRACT: The Pt(IV) complexes *trans*-$Pt(PEt_3)_2(Cl)_3(R)$ **2** (R = Cl, Ph, 9-phenanthryl, 2-trifluoromethylphenyl, 4-trifluoromethylphenyl, 3-perylenyl) were prepared by chlorination of the Pt(II) complexes *trans*-$Pt(PEt_3)_2(R)(Cl)$ **1** with $Cl_2(g)$ or $PhICl_2$. Mixed bromo−chloro complexes *trans,trans*-$Pt(PEt_3)_2(Cl)_2(Br)(R)$ (R = 9-phenanthryl, 4-trifluoromethylphenyl), *trans,cis*-$Pt(PEt_3)_2(Cl)_2(Br)$(4-trifluoromethylphenyl), *trans,trans*-$Pt(PEt_3)_2(Br)_2(Cl)(R)$ (R = 9-phenanthryl), and *trans,cis*-$Pt(PEt_3)_2(Br)_2(Cl)$(4-trifluoromethylphenyl) were obtained by halide exchange or by oxidative addition of Br_2 to **1** or Cl_2 to *trans*-$Pt(PEt_3)_2(R)(Br)$. Except for **2** (R = Ph, 4-trifluoromethylphenyl), all of the Pt(IV) complexes are photosensitive to UV light and undergo net halogen reductive elimination to give Pt(II) products, *trans*-$Pt(PEt_3)_2(R)(X)$ (X = Cl, Br). Chlorine trapping experiments with alkenes indicate a reductive-elimination mechanism that does not involve molecular chlorine and is sensitive to steric effects at the Pt center. DFT calculations suggest a radical pathway involving ^{3}LMCT excited states. Emission from a triplet is observed in glassy 2-methyltetrahydrofuran at 77 K where photoreductive elimination is markedly slowed.

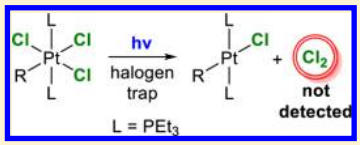

INTRODUCTION

There is growing interest in the photochemistry of transition metal complexes in relation to solar energy conversion and storage.[1−9] Several schemes to achieve conversion and storage center on splitting stable small molecules HX (e.g., H_2O, hydrogen halides) into component oxidant (X_2) and reductant (H_2).[3,6,8,10−14] A key step in these schemes is the photo-induced, expectedly endergonic reductive elimination of the oxidant (X_2) from the metal center(s) (eq 1).

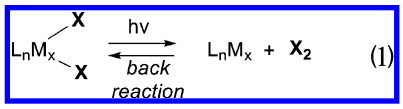

(1)

A number of apparent photoreductive eliminations of this type have been reported.[10,11,15−24] In the case of X = a halogen (Cl, Br), the reactions are generally studied using a halogen trap (alkenes or halogen-reactive solvents) to prevent the rapid back reaction, the recombination of X_2 with the reduced metal center(s). This presents a problem in that the trap renders the net reaction exergonic and opens the possibility that the trap reacts not with photoeliminated X_2 but with an excited state or reactive intermediate generated in the photolysis of the metal complex. Strong support has been found for molecular bromine (X = Br) photoelimination, although the reactions are not strongly endergonic and may have a thermal component.[19,21,23] Evidence for more strongly endergonic molecular Cl_2 photo-elimination is much weaker with Cl_2 only detected by mass spectral analysis and probably in very low quantities.[20,21] Herein, we describe our studies on net Cl_2 photoelimination in the presence of halogen traps and present evidence that the photoreactions occur not by Cl_2 photoelimination but probably by reaction of the trap with an excited state of the metal complex that acts as a chlorine atom donor.

RESULTS

Complex Synthesis and Characterization. Platinum(II) complexes, *trans*-$Pt(PEt_3)_2(R)Cl$ **1** (Scheme 1), needed for the synthesis of the targeted Pt(IV) complexes *trans*-$Pt(PEt_3)_2(R)(Cl)_3$ **2**, were prepared by three methods. The well-established oxidative addition of organochlorides (RCl) to $Pt(PEt_3)_4$ gave the R = Ph, 2-tft, 4-tft, and phen derivatives. As 3-chloroperylene is not readily available, *trans*-$Pt(PEt_3)_2$(peryl)Cl **1** (R = peryl) was instead prepared by treating *trans*-$Pt(PEt_3)_2$(peryl)Br[25] with silver triflate followed by KCl. Lastly, *trans*-$Pt(PEt_3)_2(Cl)_2$ **1** (R = Cl) was obtained by the thermal conversion of solid *cis*-$Pt(PEt_3)_2(Cl)_2$.[26]

Scheme 1

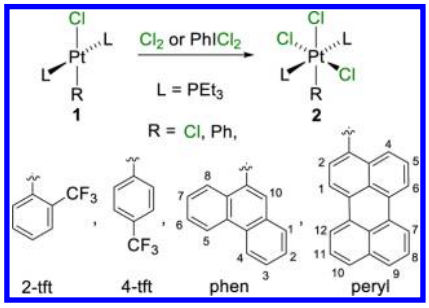

Chlorination of **1** with $Cl_2(g)$ or $PhICl_2$ yields the Pt(IV) complexes *trans*-$Pt(PEt_3)_2(R)(Cl)_3$ **2** (R = Cl, Ph, 2-tft, 4-tft, phen, peryl) (Scheme 1). For R = peryl, chlorination with Cl_2 is unselective and gives a mixture of closely related products that

Received: April 22, 2014

 © XXXX American Chemical Society dx.doi.org/10.1021/ic5009413 | Inorg. Chem. XXXX, XXX, XXX−XXX

could not be separated. These products appear to be a mixture of **2** and analogues of **2** where the perylene ring has been chlorinated, presumably in different locations and/or extent. In contrast, $PhICl_2$ selectively gives only chlorination at the Pt(II) center. However, the presence of PhI in the reaction mixture complicates isolation of **2** (R = peryl). Solvent removal triggers partial reduction of **2** to **1** (R = peryl), and white solid phenol is detected. Evidently, as concentrations increase adventitious water combines with the PhI to produce HI and phenol and the HI then reduces **2** to **1** (R = peryl). Complex **2** (R = peryl) is successfully isolated by precipitation from the reaction mixture with hexanes.

^{31}P NMR spectra of **2** show singlets with satellites in the δ 2−7 region, shifts that are about 10 units negative of those for the corresponding Pt(II) precursors **1** (δ 11−15). A similar negative shift is observed in the analogous bromo system.[19] The magnitudes of the Pt−P coupling constants are in the region expected for Pt(IV) complexes with a *trans* disposition of the PEt_3 ligands and are also similar to those observed in the analogous bromo system.[19] ^{1}H NMR spectra show the PEt_3 signals in the aliphatic region and signals for the aromatic ligands (R ≠ Cl). Complexes **2** (R = phen, peryl) yielded crystals suitable for single crystal X-ray analysis. A drawing of the phen complex is provided in Figure 1, and one for the peryl

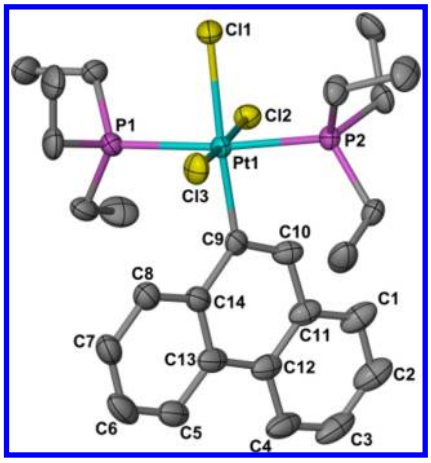

Figure 1. Solid-state structure of one of two independent molecules of **2** (R = phen, 50% probability ellipsoids, hydrogen atoms omitted). The second molecule shows a rotational disorder in the phenanthryl ring system (Supporting Information).

complex may be found in the Supporting Information. Both structures are typical of this class of complex[19] and include distortions caused by steric interactions of the *peri*-to-Pt polycyclic ring hydrogen atom (H8 on C8 in Figure 1) with the *cis* ligands (Cl3 and the P1-triethylphosphine ligand in Figure 1). Metrical parameters and other details of the structures may be found in the Supporting Information.

Mixed bromo−chloro versions of **2** are accessible by halide exchange. Thus, *trans,trans*-$Pt(PEt_3)_2(R)(Cl)_2(Br)$ **3** (R = phen, 4-tft) are obtained by treating *trans*-$Pt(PEt_3)_2(R)(Cl)_3$ with silver triflate followed by addition of tetrabutylammonium bromide (eq 2), and treating *trans*-$Pt(PEt_3)_2(R)(Br)_3$ **4** with

silver triflate followed by KCl yields *trans,trans*-$Pt(PEt_3)_2(R)(Br)_2(Cl)$ **5** (R = phen) (eq 3). The selective replacement of

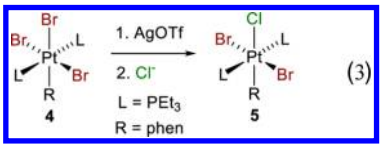

the halide ligand *trans* to the aromatic group is supported by the NMR data for **3** and **5**. Crystal structures indicate that the phenanthryl ring in this class of Pt(IV) complexes is in close contact with the *cis*-halo and phosphine ligands (see above and refs18 and 19), and therefore, the phen ring ^{1}H NMR shifts might be expected to be influenced by the identity of the *cis*-halo ligands. This is indeed the case. The ^{1}H NMR signal for H10 ($CDCl_3$), the *vicinal*-to-Pt hydrogen atom (Scheme 1 and Figure 1), appears to be most sensitive and is found at δ 8.28 for chloro complex **2** (R = phen) while that for bromo complex **4** (R = phen) appears at δ 8.59. Replacement of the *trans*-chloro ligand in **2** (R = phen) with a bromo ligand would not be expected to significantly change the shift, and this is observed; the H10 signal for **3** (R = phen) is at δ 8.26, almost exactly that of parent **2**. Likewise, replacement of the *trans*-bromo ligand in 4 (R = phen) with a chloro ligand yields an H10 shift of δ 8.54 for **5** (R = phen), essentially that of parent **4**. Replacement of the halo ligand *trans* to the carbyl ligand is expected from the strong *trans* influence of the carbyl ligand.

In the case of **3** (R = 4-tft), we have previously observed that 4-tft-ring rotation is restricted on the NMR time scale for this class of compounds.[18] Thus, if the two halide ligands *cis* to the 4-tft ligand are different, then two ^{1}H NMR signals are observed for the *ortho*-ring protons. Only one signal is observed for **3** (R = 4-tft), and the shift is similar to that of precursor **2**. Further evidence for the correct identification of **3** (R = 4-tft) is obtained from the attempted synthesis of **3** (R = 4-tft) and **5** (R = 4-tft) by halogenation of **1** (R = 4-tft) and *trans*-$Pt(PEt_3)_2$(4-tft)Br **6** (R = 4-tft) (eq 4 and eq 5). In these

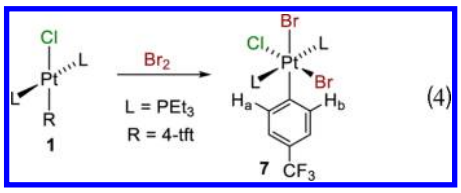

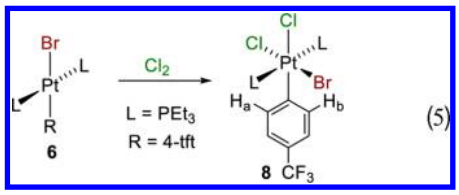

reactions, *cis*-oxidative addition is observed, and the products, *trans,cis*-$Pt(PEt_3)_2$(4-tft)$(Br)_2(Cl)$ **7** and *trans,cis*-$Pt(PEt_3)_2$(4-tft)$(Cl)_2(Br)$ **8** show two different *ortho*-ring proton signals (H_a, H_b), consistent only with slow tft-ring rotation and two different halogen ligands *cis* to the 4-tft ligand. ^{31}P NMR signals for **3** (R = 4-tft), **7**, and **8** are all singlets with satellites at different chemical shifts indicating that each is isomerically unique and not a mixture with accidentally coincident shifts.

The UV−vis absorption spectrum for **2** (R = peryl) is given in Figure 2, and those for the other derivatives are provided in the Supporting Information (Figures S88−S92). The spectrum

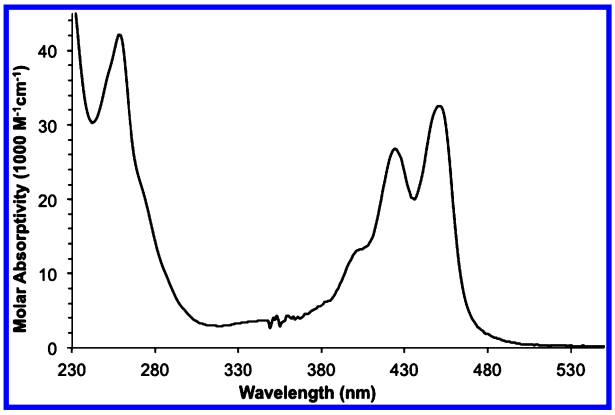

Figure 2. UV–vis absorption spectrum of *trans*-$Pt(PEt_3)_2(peryl)(Cl)_3$ **2** (R = peryl) in CH_2Cl_2.

for deep orange **2** (R = peryl) is dominated in the visible region by the peryl ligand π-to-π^* transition which shows characteristic vibronic coupling.[25] The other complexes **2** are pale yellow and absorb only weakly in the blue region. Stronger absorptions are found in the UV region, and for R = phen, the phenanthryl ligand π-to-π^* transition appears at about 300 nm with vibronic coupling (1340 cm^{-1}).[27,28] TDDFT calculations for the complexes are described below.

Photoproducts. Like their bromo analogues,[19] the chloro complexes **2** and the chloro–bromo complexes **3**, **5**, **7**, and **8** undergo photoreduction. The P-containing photoproducts depend on the complex, solvent, and the presence or absence of an added alkene (Table 1). For **2** (R = Cl), irradiation at 313 nm in the presence of excess (0.2 M) alkene yields exclusively **1** (R = Cl) and its *cis* isomer along with chlorinated alkene products (see below) (Scheme 2). If the alkene is omitted or present at low concentrations, **1** (R = Cl) is again formed but in lower yields and is accompanied by Cl_2PEt_3, $[Pt(PEt_3)(\mu\text{-}Cl)Cl]_2$, and unidentified P-containing products. Similar behavior is observed for R = 2-tft, but lower yields of **1** and greater amounts of Cl_2PEt_3 and unidentified P-containing products are obtained.

Scheme 2

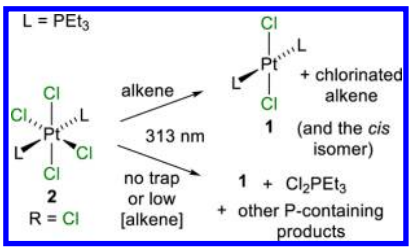

With R = phen or peryl, irradiation of **2** at 313 nm in the presence or absence of an alkene also results in photoreduction to the corresponding **1**. However, also formed is **9**, an analogue of **1** where the R group has been chlorinated (eq 6).

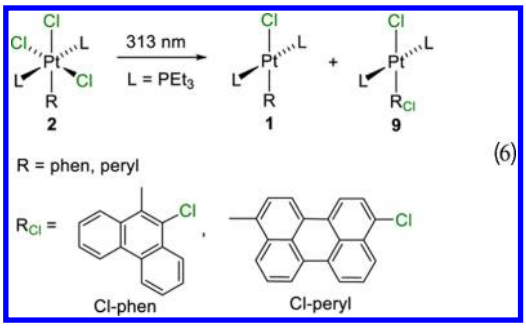

(6)

The ring-chlorination sites in **9** are shown in eq 6 and were determined by comparison of the NMR data with those for the previously reported bromo complexes.[19] A single crystal X-ray structure determination of **9** (R_{Cl} = Cl-phen) confirms the regiochemistry of the ring chlorination (Figure 3). Similar photoring bromination was reported for the bromo analogues of **2**.[19]

While **1** and **9** are produced together in the photolysis of **2** (R = phen, peryl) their ratio (**1**:**9**) is influenced by the presence of an alkene and the alkene reactivity. In the absence of an alkene, the ratio is 1:1.3 in C_6D_6 for R = phen. Adding *trans*-2-hexene suppresses ring chlorination and approximately inverts

Table 1. P-Containing Products from the Photolysis of 2 (~0.01 M) at 313 or 380 nm

			P-containing products[a]			
R (wavelength)	solvent	added trap	**1**	**9**	Et_3PCl_2	other
Cl (313 nm)	C_6D_6	none	70%[b]		11%	7% $[PtLCl_2]_2$, 12% unknown[f]
	$CDCl_3$	0.06 M TME	88%[b]		8%	4% $[PtLCl_2]_2$
	C_6D_6	0.2 M *cis*- or *trans*-2-hexene	100%[b]			
	$CDCl_3$	0.2 M TME	100%[b]			
2-tft (313 nm)	C_6D_6	0.5 M 1-hexene	42%		20%	38% unknown[f]
	C_6D_6	0.4 M TME	63%			37% unknown[f]
	CD_2Cl_2	0.3 M *trans*-3-hexene/0.3 M 1-hexene	32%		39%	29% unknown[f]
phen (313 nm)	C_6D_6	none	36%	48%		16% unknown[f]
	C_6D_6	0.2 M *trans*-2-hexene	62%	38%		
	$CDCl_3$	0.5 M 1-hexene	50%	45%		5% unknown[f]
	$CDCl_3$	0.4 M TME	89%	11%		
phen (380 nm)	$CDCl_3$	0.5 M 1-hexene		61%[c]		
	CH_2Cl_2	0.08 M 1-hexene	58%	42%		
	CH_2Cl_2	0.08 M TME	88%	12%		
	CH_2Cl_2	0.08 M TME/0.008 M pyridine	94%	6%		
	CH_2Cl_2	0.008 M pyridine	70%	16%		14% unknown[f]
peryl (380 nm)	CH_2Cl_2	none	50%[d]	50%[d]		
	CH_2Cl_2	0.2 M TME	61%[d,e]	31%[d,e]		

[a]Percent of total ^{31}P NMR integration. [b]*cis* and *trans* mixture. [c]^1H NMR yield against an internal TMS standard. [d]Ratio by ^1H NMR. [e]Isolated yield as mixture of **1** and **9**. [f]See experimental details in the Supporting Information for additional details.

dx.doi.org/10.1021/ic5009413 | Inorg. Chem. XXXX, XXX, XXX–XXX

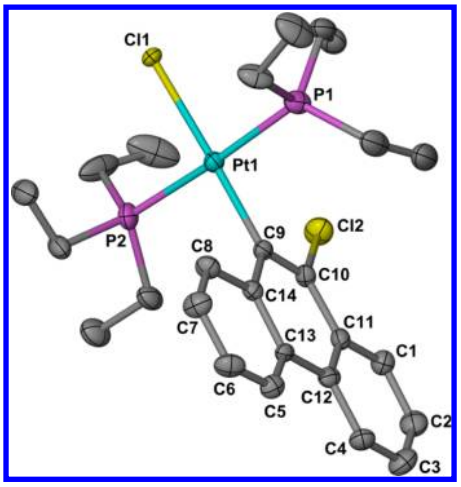

Figure 3. Solid-state structure of **9** (R_{Cl} = Cl-phen) (30% probability ellipsoids, hydrogen atoms omitted). A second orientation of one ethyl group on each phosphine ligand is not shown.

the ratio to 1.6:1. In $CDCl_3$ with 1-hexene the ratio is about 1:1, but with more electron-rich alkene TME there is only a small amount of ring chlorination, and the ratio is 8.1:1.

The photolysis of **2** with alkenes produces chlorinated alkenes (Figure 4). For R = Cl with excess (0.2 M) *cis*-2-hexene

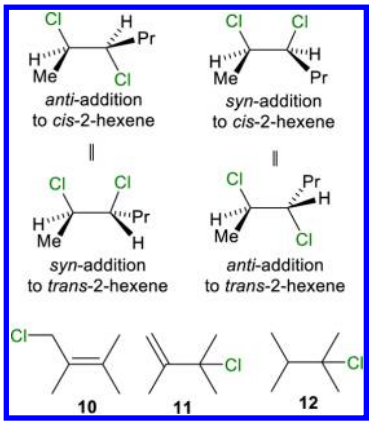

Figure 4. TME and *cis*- and *trans*-2-hexene products from the photolysis of **2**. Only one enantiomer shown for chiral 2-hexene products.

in C_6D_6, about a 1:1 mixture of the *anti*-chlorine-addition product (a racemic mixture of (2*R*,3*R*)- and (2*S*,3*S*)-2,3-dichlorohexane) and the *syn*-addition product (a racemic mixture of (2*R*,3*S*)- and (2*S*, 3*R*)-2,3-dichlorohexane) were produced in a combined yield of 51% (based on **1**). A small amount (~1%) of the remaining *cis*-2-hexene was isomerized to *trans*-2-hexene during the photolysis and cannot account for the mixture of *syn*- and *anti*-addition products. With *trans*-2-hexene a similar mixture is obtained (53% yield) with perhaps a slight favoring of the *anti*-addition product. The fate of the missing chlorine in these reactions is unknown but presumably is present in solvent (or solvent impurity) chlorination products. For **2** R = phen and *trans*-2-hexene in C_6D_6, about a 1:1 mixture of the *anti*- and *syn*-addition products is again observed. In this case, the alkene chlorination yield is only 26% (based on **1**). However, the maximum possible yield is 62%, since 38% of the Cl_2 from **2** has gone to phenanthryl ring chlorination in the formation of **9**.

With TME and R = Cl, high combined yields (90−100%) of the two chlorination products 1-chloro-2,3-dimethyl-2-butene **10** (29−30%) and 3-chloro-2,3-dimethyl-1-butene **11** (60−70%) are obtained. Both of these chlorination products must be accompanied by HCl formation, and the TME−HCl addition product, 2-chloro-2,3-dimethylbutane **12**, is therefore also present. TME chlorination products are the same for R = phen, but the combined yield decreases to 45%. As with hexene, part of the decrease can be attributed to chlorine loss (11%) to ring chlorination.

The reaction of Cl_2 with excess TME and *cis*- and *trans*-2-hexene was examined for comparison with the photoreactions. For TME the exclusive products are 3-chloro-2,3-dimethyl-1-butene and 2-chloro-2,3-dimethylbutane, as previously reported.[29] For *cis*- and *trans*-2-hexene, the *anti*-addition products are the only detected products.

To further investigate the nature of the photoreduction of **2**, a competition experiment[30] was conducted in which **2** (R = Cl, 2-tft) were photolyzed at 313 nm with an excess 1:1 mixture of 1-hexene and *trans*-3-hexene in CD_2Cl_2 (Scheme 3).

Scheme 3

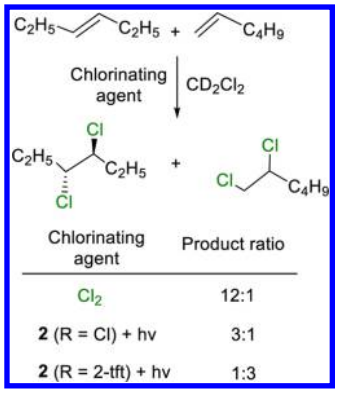

Chlorinating agent	Product ratio
Cl_2	12:1
2 (R = Cl) + hv	3:1
2 (R = 2-tft) + hv	1:3

The resulting product ratio of 3,4-*trans*-dichlorohexane and 1,2-dichlorohexane was 3:1 for R = Cl and 1:3 for R = 2-tft. A 12:1 ratio was obtained with Cl_2 as the chlorinating agent. (A solution of Cl_2 was slowly added to a rapidly stirred solution of the alkene mixture in order to approximate the conditions that would be obtained if molecular Cl_2 is photoeliminated from the complexes.)

Photokinetics. The photolyses of **2** (R = Cl, phen, 2-tft) and TME at 380 nm in $CDCl_3$ were monitored by ^{31}P NMR spectroscopy. This wavelength was chosen in an attempt to avoid absorbance by photoproduct **1** and ring-chlorination product **9** (R_{Cl} = Cl-phen). In addition, absorbance at this wavelength by **2** is low such that the reaction is not limited by the photon flux but only by the concentration of **2**. Under these conditions the rate of the photoreaction should be first order in **2**. As expected, plots of the concentration of **2** against time for R = Cl and 2-tft are first order, and log plots give straight lines (Supporting Information Figures S93 and S94). In contrast, the plot for R = phen does not show first-order behavior (Figure 5). Instead, the photoreaction shows a low initial rate (slope = −0.092) that increases as the reaction progresses reaching a final rate that is more than 4 times higher (slope = −0.39) than the initial rate.

Such a rate increase is suggestive of a product-catalyzed reaction (autocatalysis).[31,32] The photoreaction was therefore repeated with 1 molar equiv of photoproduct **1** (R = phen)

dx.doi.org/10.1021/ic5009413 | Inorg. Chem. XXXX, XXX, XXX−XXX

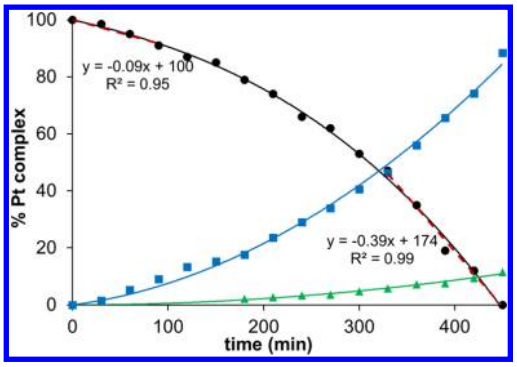

Figure 5. Photolysis of **2** (R = phen) (9 mM) with TME (90 mM) in dichloromethane at 380 nm: black circles for **2**, blue squares for **1** (R = phen), green triangles for ring-chlorinated **9** (R_{Cl} = Cl-phen). The solid lines are polynomial fits to the data and are intended only to aid the eye. Red dashed lines are linear fits (with equations) at the beginning and end of the reaction.

added at the beginning of the reaction. A linear plot of the concentration of **2** (R = phen) against time is then observed (Figure 6) with a reaction rate that is near that of the final rate

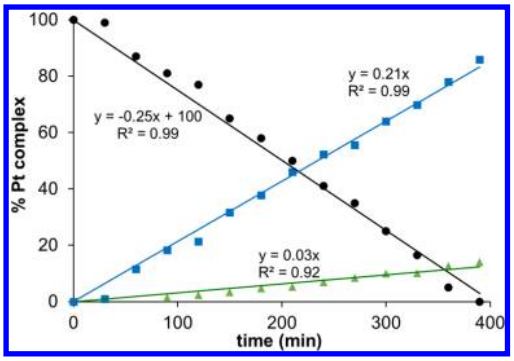

Figure 6. Photolysis of **2** (R = phen) (9 mM) with TME (90 mM) and **1** (R = phen) (9 mM) in dichloromethane at 380 nm: black circles for **2** (R = phen), blue squares for **1** (R = phen), green triangles for ring-chlorinated **9** (R_{Cl} = Cl-phen). The lines are linear fits to the data with fixed intercepts of 0 or 100%.

of the reaction without added **1** (R = phen). These results indicate that photoproduct **1** is a catalyst for the photoreaction. Also of note is that the addition of **1** at the beginning of the reaction does not alter the final Pt-containing product distribution. In both reactions the yield of the ring chlorination product **9** (R_{Cl} = Cl-phen) is about 10%. Thus, whatever the role of **1** in accelerating the reaction, it does not affect the ring chlorination amount. Similar results are obtained using 1-hexene as the chlorine trap (Supporting Information Figures S95 and S96) but with a ~40% yield of **9** (R_{Cl} = Cl-phen). A close inspection of the UV−vis absorption data for **1** (R = phen) reveals that the extinction coefficient near 380 nm is not zero but approximately half that of **2** (R = phen). We therefore conclude that **1** (R = phen) is an efficient sensitizer for excitation of **2** (R = phen) into the photochemically active excited state (most likely the lowest-energy triplet, see below).

Solid-State Photolyses. Previously it was found that solid-state samples of Au and Pt bromo complexes photoeliminate chemically detectable amounts of Br_2 into the gas phase.[19,21] In contrast, photolysis of solid-state samples of chloro complexes did not release chemically detectable amounts of Cl_2, although an undetermined quantity was detected by mass spectrometry.[20,21] Solid samples of **2** (R = Cl, phen) were photolyzed at 313 nm in a vacuum with LN_2 trapping of any photoeliminated Cl_2 into a 1-hexene or TME solution. Although photoreduction of **2** was observed, no alkene−chlorination products were detected leading us to conclude that no significant amounts of Cl_2 are evolved in the photolysis of solid **2**. No effort was made to detect Cl_2 by mass spectrometry.

Elimination Stereoselectivity. To explore the halogen photoelimination stereoselectivity (*cis* or *trans*), *trans,trans*-$Pt(PEt_3)_2(phen)(Cl)_2(Br)$ **3** (R = phen) and *trans,trans*-$Pt(PEt_3)_2(phen)(Br)_2(Cl)$ **5** (R = phen) were separately photolyzed with excess TME at 313 nm in $CDCl_3$. Under these conditions (Table 1) the photoreduction of parent **2** (R = phen) is clean with the only P-containing product being **1** (R = phen). This proved also true for **3** and **5** (R = phen), and the only detected P-containing products are $Pt(PEt_3)_2(Cl)$-(phen) **1** (R = phen) and $Pt(PEt_3)_2(Br)(phen)$ **6** (R = phen). For **5** (R = phen), bromo complex **6** (R = phen) is the exclusive Pt-containing product suggesting a highly selective *cis*-elimination of BrCl (eq 7). Complex **3** (R = phen) gives a

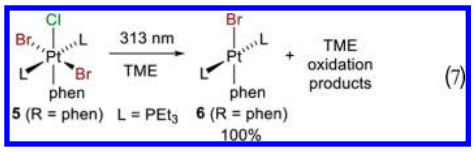

mixture of **1** (R = phen) and **6** (R = phen), with **1** (R = phen) formed in 86% yield and **6** (R = phen) in 14% yield (eq 8).

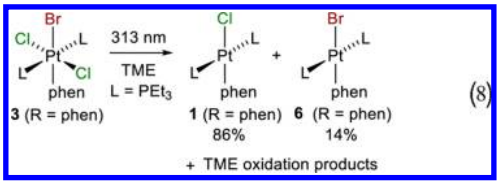

This would suggest lower *cis*-elimination selectivity; however, **6** (R = phen) is likely formed from the reaction of **1** (R = phen) with HBr from TME oxidation. As with **2**, some of the TME products (Table 2) require the formation of HBr and HCl, and in separate experiments we find that **1** (R = phen) reacts rapidly with HBr,[33] even in the presence of TME, to produce **6** (R = phen). In contrast, **6** (R = phen) does not react at all with HCl. Thus, **1** (R = phen) may be the exclusive initial product of *cis*-photoelimination, but some (14%) reacts with HBr to produce **6** (R = phen). TME products from the photolysis of **3** (R = phen) are listed in Table 2 and are formed in similar yields in the photolysis of **5** (R = phen).

We also hoped to examine the photoelimination stereochemistry in the mixed bromo−chloro complexes **3** (R = 4-tft) and **7**, but the photoeliminations are complicated by photoisomerization and halide exchange. Consistent with a preference for *cis* elimination, photolysis of **3** (R = 4-tft) with 1-hexene gives 70% **1** (R = 4-tft) and 30% **6** (R = 4-tft). However, monitoring the reaction reveals that *trans*-dichloro **3** (R = 4-tft) is partially photoisomerized to *cis*-dichloro **8**. Photolysis of pure **8** gives essentially the same final **1** (R = 4-tft)-to-**6** (R = 4-tft) ratio as **3** (R = 4-tft), but again, reaction monitoring indicates some isomerization to **3** (R = 4-tft) and also formation of trichloro **2** (R = 4-tft). As a result, it is not possible to establish the photoelimination stereochemistry for the R = 4-tft system.

Quantum Yields. Quantum yields for the photoreductions of **2** are listed in Table 3. The highest yield (58%) is for

Table 2. Photolysis Product Yields[a] for *trans,trans*-$Pt(PEt_3)_2(phen)(Cl)_2(Br)$ 3 with 2,3-Dimethyl-2-butene (TME)

Products	Yield
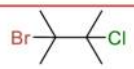 **13**	16%
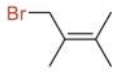 **14**	24%
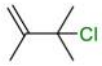 **10**	17%
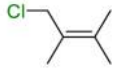 **11**	12%
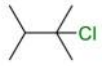 **12**	26%
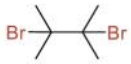 **15**	3%
Cl atom yield	71%
Br atom yield	60%

[a]^{1}H NMR yields relative to **1** (R = phen) + **6** (R = phen).

Table 3. Quantum Yields for Photoreduction of 2 at 313 nm

R	solvent	trap	[trap] (M)	[Pt] (mM)	QY (%)[a]
2-tft	DCM[b]	TME	0.2	0.58	58 ± 2
Cl	benzene	1-hexene	0.05	0.13	24 ± 1[c]
Cl	benzene	TME	0.017	0.14	25 ± 3[c]
Cl	DCM	TME	0.046	0.13	19 ± 1[c]
Cl	DCM	TME	0.15	0.13	21 ± 1[c]
Cl	DCM	TME	0.62	0.14	20 ± 2[c]
phen	DCM	TME	0.15	0.25	1.0 ± 0.2
peryl	DCM	1-hexene	0.13	0.16	9.4 ± 0.2
peryl	DCM	1-hexene	0.13	0.12	2.6 ± 0.9[d]
peryl	DCM	1-hexene	0.13	0.12	0[e]

[a]Average of three runs at three monitoring wavelengths. [b]DCM = dichloromethane. [c]Single monitoring wavelength (see experimental details in the Supporting Information). [d]At 380 nm. [e]At 400 nm.

2 (R = 2-tft) and is the highest yet reported for net chlorine photoelimination from a transition metal chloro complex. (The highest previous yield of 38% is claimed by the dinuclear complex $Pt_2(tfepma)_2Cl_6$, tfepma = $[P(CF_3CH_2O)_2]_2NMe$.[20]) Yields are somewhat lower for R = Cl and are solvent dependent. The best yields are obtained in benzene and are nearly the same in the presence of TME and 1-hexene. Lower yields are observed for dichloromethane and are essentially independent of TME concentration over the range examined. The yields drop considerably for R = phen and peryl, and the peryl complex shows an excitation wavelength dependence. Despite strong absorption in the blue region (Figure 2) no photoreduction is observed at 400 nm. Decreasing the photolysis wavelength to 380 nm gives slow conversion with a quantum yield of 2.6%. The photoreduction is accompanied by strong visible peryl ligand emission.[25] (None of the other complexes **2** display visible room-temperature photoemission in solution.) Decreasing the photolysis wavelength further to 313 nm decreases the emission and increases the reaction quantum yield to 9.4%. Emission spectroscopy (Figure 7) confirms the emission decrease and indicates a 5-fold reduction on going from 380 to 313 nm, nearly matching the 4-fold reaction quantum yield increase.

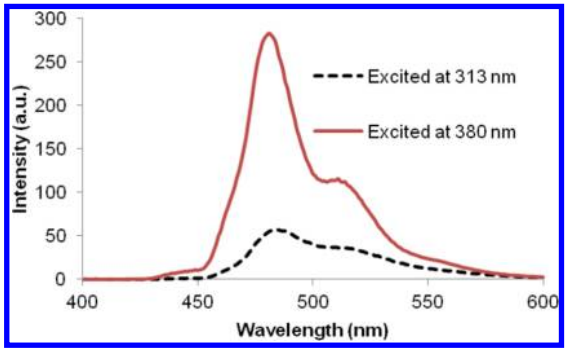

Figure 7. Photoemission spectrum of *trans*-$Pt(PEt_3)_2(peryl)(Cl)_3$ **2** (R = peryl) in CH_2Cl_2. Solid red line for 380 nm excitation and dashed black line for 313 nm excitation.

Low-Temperature Photoemission. As mentioned above, only the peryl complex shows photoemission in solution at room temperature. However, the other complexes **2** (R = Cl, 2-tft, 4-tft, phen) do show photoemission in a 2-methyltetrahydrofuran glass at 77 K (Table 4). The emission colors range from yellow to orange with the brightest emission seen for R = Cl. The emission spectra are given in Figure 8 and show broad (fwhm =2150 to 3060 cm^{-1}), unstructured emission bands at 580−590 nm. (The differing emission colors appear to be due more to the degree of tail off into the red than to differing maxima.) The same emission bands are observed with 320, 380, or 390 nm excitation and show exponential decay with mean lifetimes of 66−109 μs. An emission band is also observed at ∼480 nm for R = phen and is assigned to phenanthrenyl ligand phosphorescence.[34] Along with emission turn-on in the frozen matrix there is a strong decrease in the photoreduction of **2** with conversion rates that are reduced by

Table 4. Emission Data for 2 in 2-Methyltetrahydrofuran Glass at 77 K (380 nm excitation)

R	λ_{max} (nm)	fwhm (cm^{-1})	lifetime (μs)[a]
Cl	590	2150	84
2-tft	585	2660	66
4-tft	605	3060	64
phen[b]	580	∼3000	109

[a]Errors are estimated to be 1 μs or less. [b]Probable phen ligand emission observed at ∼480 nm.

dx.doi.org/10.1021/ic5009413 | Inorg. Chem. XXXX, XXX, XXX−XXX

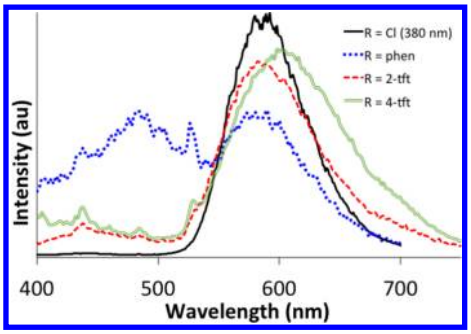

Figure 8. Photoemission spectrum of *trans*-$Pt(PEt_3)_2R(Cl)_3$ **2** (11−17 mM) in 2-methyltetrahydrofuran glass at 77 K with 390 or 380 nm excitation. Intensity traces are scaled to minimize overlap and do not represent relative intensities.

at least a factor of 3 from the room-temperature rates. Of note is that the amount of ring chlorination for R = phen is reduced by at least 50% from that in 2-methyltetrahydrofuran at room temperature suggesting that constraints imposed by the rigid solvent matrix inhibit ring chlorination.

DFT Modeling. Model complexes where the PEt_3 ligands are replaced with PMe_3 ligands were used in all calculations and are given the same number as the experimental complexes (where applicable) but with a prime added. Thus, model complexes for **2** are designated as **2′** and have the formula *trans*-$Pt(PMe_3)_2(Cl)_3R$.

Calculated (M06) gas-phase molecular chlorine reductive-elimination enthalpies and free energies for **2′** (R = Cl, phen, 2-tft, 4-tft) are shown in Table 5. As expected, the eliminations

Table 5. Calculated (M06, Gas Phase, 298 K, 1 atm) ΔH, ΔG, and $T\Delta S$ Values (kcal/mol) for Chlorine Reductive Elimination from *trans,trans*-$Pt(PMe_3)_2Cl_2(R)$ 2′ (R = Cl, phen, 2-tft, 4-tft)

R	ΔH	$T\Delta S^a$	ΔG^a
Cl	41.1	10.9	30.2
phen	41.1	14.0	27.1
2-tft	33.2	13.2	20.1
4-tft	50.0	10.6	39.4

[a] ΔG and $T\Delta S$ values are expected to decrease by about 3 kcal/mol when corrected for the smaller entropy increase in solution as compared to the gas phase.[19,35,36]

are endergonic (22−39 kcal/mol), and the free energy values are 2−4 times greater than for related bromo complexes.[19] Despite the expectedly greater electron density on the Pt centers in the carbyl complexes, only for R = 4-tft is the reductive elimination enthalpy greater than that for the expectedly less-electron-rich chloro complex (R = Cl). The low values for the R = phen, 2-tft complexes can be attributed to the strong steric interaction of the *peri*-to-Pt, phenanthryl-hydrogen atom (H8), and the 2-CF_3 group in **2′** (see above and ref 19) which is at least partly relieved in the square planar products **1′**. Also of note is the more favorable entropy term ($T\Delta S$) for R = phen and 2-tft, which are 2−3 kcal/mol more favorable than for R = Cl and 4-tft. The more favorable entropy term for R = phen and 2-tft is attributed to an increase in rotational motion of the R group on going from very crowded 6-coordinate Pt(IV) to 4-coordinate Pt(II).

We focus first on **2** (R = Cl) as this is the simplest photoactive system and does not have the complication of an aromatic group. Calculated vertical electronic transitions (TDDFT, CAM-B3LYP) for **2′** (R = Cl) in dichloromethane (pcm) using the gas-phase optimized (M06) structure (see below) are shown in Table 6. The calculated transition energies and oscillator strengths are compared to the experimental UV−vis absorption spectrum of **2** (R = Cl) in Figure 9.

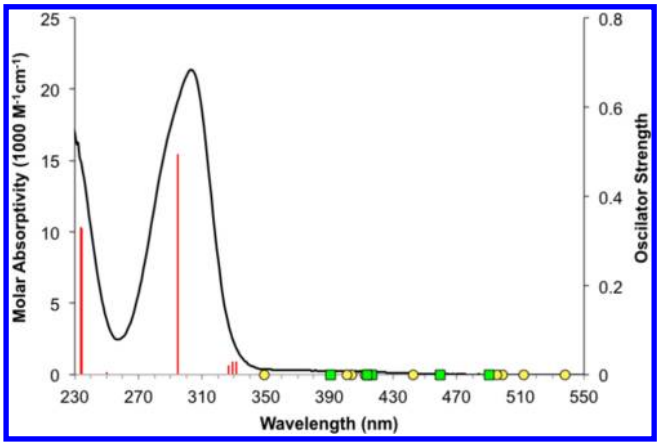

Figure 9. UV−vis absorption spectrum of *trans*-$Pt(PEt_3)_2(Cl)_4$ **2** (R = Cl) in dichloromethane (black line) and TDDFT (CAM-B3LYP, pcm) vertical transitions for *trans*-$Pt(PMe_3)_2(Cl)_4$ **2′** (R = Cl) (red vertical lines, height corresponds to the oscillator strength) in dichloromethane. Yellow circles mark calculated triplet transitions, and green squares mark calculated dark (oscillator strength <0.01) singlet transitions at >350 nm.

The match is quite good with excellent correspondence of maxima and minima and relative intensities. The five lowest-energy singlet transitions (Table 6 and Figure 9) are dark (oscillator strength ∼0) but should be accessible through internal conversion from bright, higher-energy, singlet states. Matching triplet transitions for the dark singlet transitions are found at somewhat lower energy with a slightly different ordering where the first and second transitions are switched for the triplets (Table 6 and Figure 9). The destination orbital for all five transitions is the LUMO (Figure 10), which is Pt−Cl

Table 6. Five Lowest TDDFT (CAM-B3LYP, pcm) Vertical Transitions for *trans*-$Pt(PMe_3)_2(Cl)_4$ 2′ (R = Cl) in Dichloromethane[a]

singlets			triplets			
cm^{-1}	nm	contribution (>5%)	cm^{-1}	nm	contribution (>5%)	S−T gap cm^{-1} (eV)
20 393	490	HOMO → LUMO (99%)	19 523	512	HOMO → LUMO (97%)	870 (0.11)
21 770	459	H-4 → LUMO (93%)	18 578	538	H-4 → LUMO (91%)	3192 (0.40)
24 009	416	H-2 → LUMO (88%)	20 054	498	H-2 → LUMO (83%)	3955 (0.49)
24 156	413	H-3 → LUMO (90%)	20 185	495	H-3 → LUMO (85%)	3971 (0.49)
25 593	390	H-1 → LUMO (95%)	22 605	442	H-1 → LUMO (89%)	2988 (0.37)

[a] All singlets are "dark" (oscillator strength <0.001).

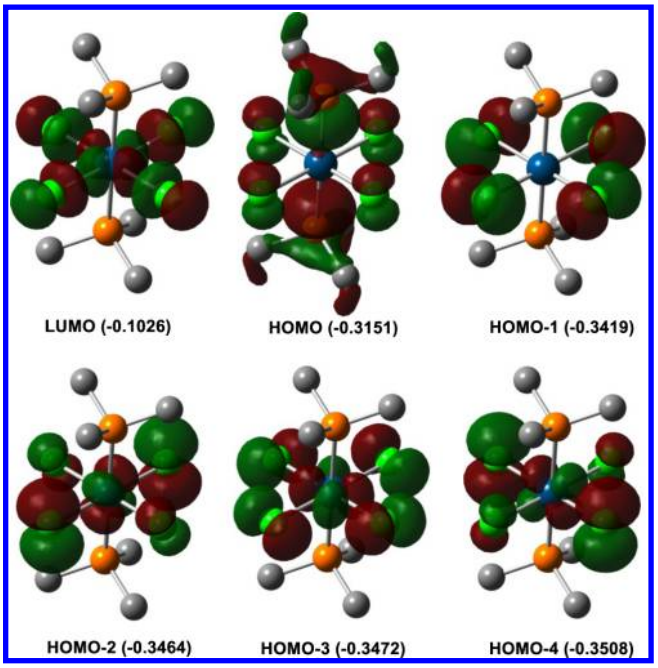

Figure 10. Selected orbitals (isovalue = 0.04 e/Å^3, CAM-B3LYP) for *trans*-Pt(PMe$_3$)$_2$(Cl)$_4$ **2′** (R = Cl) in dichloromethane (pcm). Hydrogen atoms omitted. Atom colors: blue = Pt, orange = P, green = Cl, gray = C. Numbers in parentheses are orbital energies in Hartrees.

antibonding and, in pseudo-octahedral symmetry, can be identified as a $d_{x^2-y^2}$, e_g*-like orbital. (The other member of the e_g*-like set, the d_{z^2} orbital, is the LUMO + 1 and is oriented along the P−Pt−P axis at higher energy due to the stronger phosphine ligand field.) The departure orbitals are predominantly (88% or greater) the HOMO through HOMO − 4. The HOMO is mostly phosphine ligand based with some contribution from Cl lone-pair p-orbitals, while the HOMO − 1 is purely Cl lone-pair. HOMO − 2, − 3, and − 4 are also Cl lone-pair based but with some Pt d-orbital contribution (d_{xy}-, d_{xz}-, d_{yz}-like orbitals). Thus, the five lowest-energy transitions (triplets and singlets) involve electron density transfer from ligand-based (mostly Cl) orbitals to a Pt−Cl antibonding orbital. The small energy gap between the singlet and matching triplets (especially the HOMO−LUMO transitions) suggests facile intersystem crossing and the likely involvement of a triplet excited state in the photochemistry of these systems. Singlet-to-triplet intersystem crossing occurs in less than 150 fs in $PtBr_6^{2-}$.[37]

Gas-phase relaxed triplets derived from **2′** were calculated (M06). For R = Cl, two triplet minima were located, and the structures are shown in Figure 11. Triplet **2′^{T1}** (R = Cl) is lowest and lies 39.9 kcal/mol (40.8 kcal/mol in dichloromethane) above singlet **2′**. An increase in one Pt−Cl distance (Pt−Cl1) from 2.40 Å in **2′** (R = Cl) to 2.69 Å in **2′^{T1}** (R = Cl) is evident. Along with the increased Pt−Cl distance is a bending of the *cis*-Cl atoms, Cl2 and Cl4, toward the elongated position giving a Cl2−Pt−Cl4 angle of 154°. The other Pt−Cl distances have also lengthened but not to the degree observed for Pt−Cl1. In contrast, the Pt−P bonds have slightly shortened from 2.42 Å in **2′** (R = Cl) to 2.40 Å in **2′^{T1}** (R = Cl), and the phosphine ligands have bent slightly away from Cl1 toward Cl3, giving a P1−Pt−P2 angle of 175°.

Triplet **2′^{T2}** (R = Cl) is 42.2 kcal/mol (42.8 kcal/mol in dichloromethane) above **2′** placing it about 2 kcal/mol higher

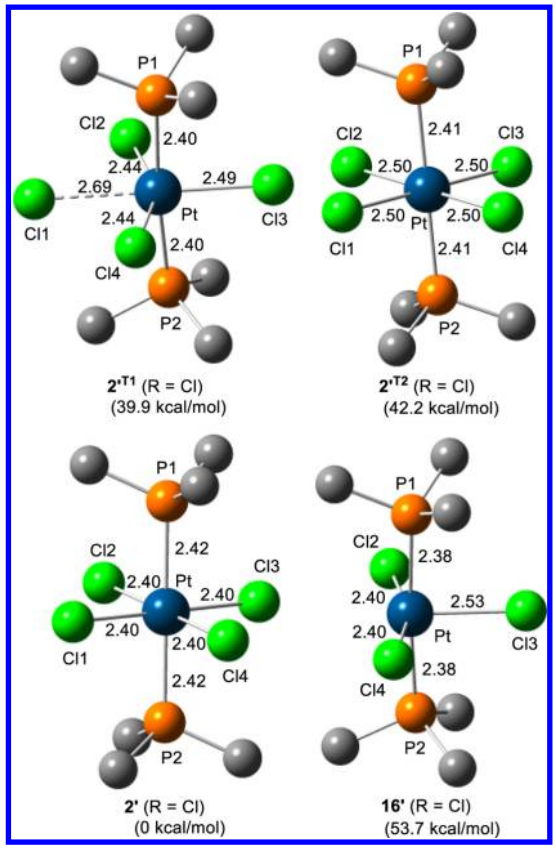

Figure 11. Singlet **2′**, triplet **2′^{T1}** (R = Cl) and **2′^{T2}** (R = Cl), and doublet **16′** (R = Cl) structures from *trans*-Pt(PMe$_3$)$_2$(Cl)$_4$ **2′** (R = Cl). Hydrogen atoms omitted. Distances in angstroms, gas-phase energies above singlet **2′** (R = Cl) in parentheses, and that for **16′** (R = Cl) includes a Cl radical.

in energy than triplet **2′^{T1}** (R = Cl). There is again Pt−Cl bond elongation from singlet **2′**, but all Pt−Cl distances are the same and at 2.50 Å are close to the average of those (2.52 Å) in **2′^{T1}** (R = Cl). At first glance, the symmetry of both **2′^{T2}** (R = Cl) and singlet **2′** is D_{4h}. Closer inspection reveals a tilt of the P1−Pt−P2 axis (both P1−Pt−P2 angles are 180°) in both structures such that this axis is not perpendicular to the plane containing Pt, Cl1, Cl2, Cl3, and Cl4. The tilt is more severe in triplet **2′^{T2}** (R = Cl) but can be attributed in both complexes to steric interactions of the PMe$_3$-methyl groups with the Cl atoms. In the direction of the tilt, a methyl group on each phosphine ligand nestles between two *cis*-Cl atoms (C1 and Cl2 for P1, Cl3 and Cl4 for P2), relieving steric interactions between the other methyl groups and Cl atoms which are directly under them. The greater tilt in **2′^{T2}** (R = Cl) is apparently allowed by the longer Pt−Cl distances, which open the gaps between the Cl atoms for deeper nestling of the methyl groups. In both complexes the average C···Cl distance for the methyl groups in contact with the Cl atoms is identical.

Mulliken atomic spin densities (see ref 38 for a review of spin-density distribution in transition metal complexes) for the two triplets are given in Table 7. Of note is the larger spin density on the Cl atoms in **2′^{T1}** (R = Cl). This is especially so for Cl1, the Cl atom with the very long distance to Pt, and suggests strong Cl radical character and the possibility that this triplet is a good Cl atom donor. The distribution is also consistent with a triplet that might be derived from Cl-to-Pt charge-transfer originating from HOMO − 1 (Figure 10).

Table 7. Triplet and Doublet Mulliken Atomic Spin Densities (Gas Phase) for R = Cl[a]

atom	$2'^{T1}$ (R = Cl)	$2'^{T2}$ (R = Cl)	16′ (R = Cl)
Pt	0.622	0.865	0.550
Cl1	0.484	0.289	
Cl2	0.345	0.287	0.063
Cl3	0.209	0.289	0.320
Cl4	0.345	0.287	0.063
Cl total	1.383	1.152	0.446

[a]Spin densities greater than 0.01.

The much greater spin density on Pt in $2'^{T2}$ (R = Cl) suggests that this triplet may instead originate from HOMO − 2, HOMO − 3, or HOMO − 4 or a combination of these. The low spin density on the P atoms (<0.01) in both of these triplets is not consistent with contributions from a HOMO-to-LUMO transition. Since HOMO-to-LUMO transition is the lowest-energy vertical transition, either we have not found the lowest-energy relax triplet structure or there is a reordering in the excited states in the relaxation process. Alternatively, either the vertical-transition energy or the triplet-state energy ordering is incorrect.

Complete dissociation of a Cl atom from the triplets was examined by optimizing doublet *trans*-$Pt(PMe_3)_2(Cl)_3$ **16′** (R = Cl) (Figure 11). The doublet and a Cl atom are 53.7 kcal/mol (51.6 in dichloromethane) above singlet **2′** (R = Cl) or 11.5 kcal/mol (10.8 in dichloromethane) above $2'^{T2}$ (R = Cl) and 13.8 kcal/mol above $2'^{T1}$ (R = Cl). Of note is that the approximately square-pyramidal geometry of doublet **16′** (R = Cl) is very close to that of triplet $2'^{T1}$ (R = Cl) after removal of Cl1 (Figure 11). Thus, the Pt−Cl1 bond in $2'^{T1}$ (R = Cl) and $2'^{T2}$ (R = Cl) is very weak, and the triplets should be a very good Cl atom donor with minimal geometric rearrangement for triplet $2'^{T2}$ (R = Cl).

Removal of a Cl atom from **16′** (R = Cl), though not as facile as for the triplets, requires only 29.5 kcal/mol (31.5 kcal/mol in dichloromethane). With a reported Cl_2 bond enthalpy of 58.0 kcal/mol[39] and a calculated (M06) ΔG of 53.0 kcal/mol, it seems a Cl radical is capable of abstracting a Cl atom from **16′** (R = Cl) with formation of Cl_2. Abstraction of the Cl atom by a carbon radical would be even more favorable. Spin densities in **16′** (R = Cl) show the largest Cl spin density (0.32) on axial Cl3 (Table 7) suggesting that this would be the Cl atom to be removed. However, isomerization in square-pyramidal complexes is usually a low-energy process, and transition state **17′** (R = Cl) for axial−equatorial Cl exchange in **16′** (R = Cl) is indeed only 0.8 kcal/mol above **16′** (R = Cl). Applying the Eyring equation gives a picosecond room-temperature lifetime for axial−equatorial Cl atom exchange in **16′** (R = Cl) indicating that abstraction of any of the Cl atoms is possible after rearrangement to an axial position.

In contrast to **2′** (R = Cl), the TDDFT results for **2′** (R = 4-tft, 2-tft, phen) do not fully match the experimental spectra (Figure 12, R = phen; Supporting Information Figure S99, R = 4-tft; Supporting Information Figure S100, R = 2-tft). The match is good for the weak transitions in the low-energy region (>300 nm), but the energies of the high-intensity transitions deeper in the UV appear to be overestimated. In addition, orbital compositions (Table 8 and Supporting Information Tables S26−S29) for the first five transitions are more complex than for R = Cl, and most are without dominant (>80%) contributions. For R = phen (Table 8), only four of the five

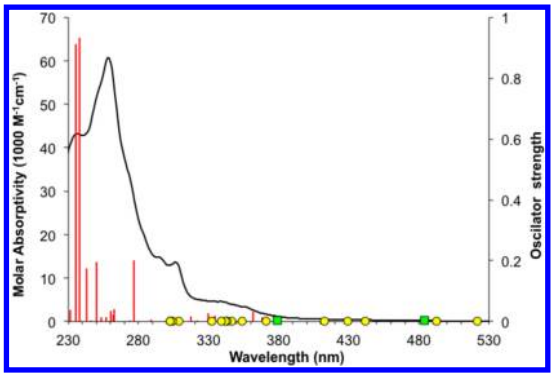

Figure 12. UV−vis absorption spectrum of *trans*-$Pt(PEt_3)_2(Cl)_3$(phen) **2** (R = phen) in dichloromethane (black line) and TDDFT (CAM-B3LYP, pcm) vertical transitions for *trans*-$Pt(PMe_3)_2(Cl)_3$(phen) **2′** (R = phen) (red vertical lines, height corresponds to the oscillator strength). Yellow circles mark calculated triplet transitions (>300 nm), and green squares mark calculated dark (oscillator strength <0.01) singlet transitions (>370 nm).

lowest-energy singlet transitions find an approximate match in the five lowest-energy triplet transitions. With the exception of the second triplet at 492 nm, all of the transitions have the LUMO as the destination orbital. As for **2′** (R = Cl), the LUMO (Figure 13) is predominantly an e_g*-like Pt−Cl antibonding orbital, but in this case it can be described as a Pt d_{z^2} based orbital directed along the Cl−Pt−Cl axis. (The higher-lying LUMO + 1 is a Pt dx^2-y^2, e_g*-like orbital in the phen and phosphine ligand plane.) The HOMO and HOMO − 1 are almost pure phen π orbitals, and the HOMO − 2 through HOMO − 8 are similar to the orbitals for **2′** (R = Cl) (large contributions from Cl lone-pair orbitals) with some contribution from phen ligand π orbitals. Thus, the excitation picture is similar to that for **2′** (R = Cl) with electron density transfer from primarily ligand-based orbitals to an antibonding Pt−Cl orbital, but in contrast to **2′** (R = Cl) the antibonding orbital is directed along the Cl−Pt−Cl axis and there is significant involvement of the phen π system. Similar conclusion can be made for **2′** (R = 4-tft, 2-tft) (Supporting Information Tables S28 and S29, Figures S101 and S103).

Relaxed triplet calculations for **2′** (R = 4-tft) located three different structures (Figure 14). Structure $2'^{T1}$ (R = 4-tft), at 43.2 kcal/mol above the singlet, is similar to $2'^{T1}$ (R = Cl) in having a unique elongated Pt−Cl1 bond (2.96 Å) along a Cl−Pt−Cl axis, slightly longer other Pt−Cl bonds, and slightly shorter Pt−P distances relative to singlet **2′** (R = 4-tft). In addition, the Pt−C distance is slightly shorter, and the tft ring is rotated into the Pt, C1, Cl1, Cl2, Cl3 plane. The other two triplets, $2'^{T2}$ (R = 4-tft) and $2'^{T3}$ (R = 4-tft), resemble $2'^{T2}$ (R = Cl) in having equal or nearly equal Pt−Cl distances along the Cl−Pt−Cl axis. All other distances and the orientation of the tft ring in $2'^{T2}$ (R = 4-tft) are essentially the same as in $2'^{T1}$ (R = 4-tft), as is the energy (42.7 kcal/mol above the singlet). In contrast, $2'^{T3}$ (R = 4-tft) is significantly higher in energy (47.1 kcal/mol above the singlet) and has the tft ring rotated out of the Pt/Cl plane. The Pt−C distance is also reduced, and as shown below, this ring orientation and the shorter Pt−C distance is likely associated with high tft-ring spin density. As with R = Cl, complete loss of a Cl atom from all of the triplets is relatively facile with doublet, square-pyramidal *trans*-$Pt(PMe_3)_2R(Cl)_2$ **16′** (R = 4-tft) and a Cl atom 16 kcal/mol above $2'^{T1}$ (R = 4-tft) and $2'^{T2}$ (R = 4-tft) and 12 kcal/mol

Table 8. Five Lowest-Energy TDDFT (CAM-B3LYP, pcm) Vertical Transitions for *trans*-Pt(PMe$_3$)$_2$R(Cl)$_3$ 2′ (R = phen) in Dichloromethane

singlets				triplets			
cm^{-1}	nm	osc	contribution (>5%)	cm^{-1}	nm	contribution (>5%)	T−S gap cm^{-1}
20 664	484	0.0034	HOMO → LUMO (86%)	19 178	521	HOMO → LUMO (74%)	1486
						H-7 → LUMO (7%)	
				20 304	492	HOMO → L+2 (65%)	
						H-1 → L+3 (23%)	
26 393	379	0.0044	H-7 → LUMO (53%)	22 638	442	H-7 → LUMO (49%)	3755
			H-4 → LUMO (9%)			H-4 → LUMO (9%)	
			H-2 → LUMO (7%)			H-8 → LUMO (8%)	
						H-2 → LUMO (7%)	
						HOMO → LUMO (6%)	
27 161	368	0.0147	H-8 → LUMO (64%)	23 290	429	H-8 → LUMO (76%)	3871
			H-2 → LUMO (27%)			H-2 → LUMO (11%)	
27 646	362	0.0329	H-2 → LUMO (51%)	24 240	412	H-2 → LUMO (59%)	3406
			H-8 → LUMO (22%)			H-7 → LUMO (11%)	
			H-7 → LUMO (9%)			H-3 → LUMO (7%)	
			H-3 → LUMO (8%)				
29 443	340	0.0046	H-1 → LUMO (76%)				
			H-3 → LUMO (14%)				

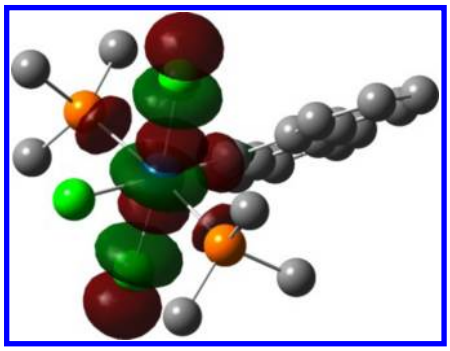

Figure 13. LUMO (isovalue = 0.04 e/Å^3, CAM-B3LYP, pcm) for *trans*-Pt(PMe$_3$)$_2$(Cl)$_3$(phen) 2′ (R = phen) in dichloromethane. Atom colors: blue = Pt, orange = P, green = Cl, gray = C.

above **2′^{T3}** (R = 4-tft). Although two doublet structures are possible with equatorial and axial 4-tft ligand, only the equatorial structure is a minimum. Exchange between the axial and equatorial Cl atoms in doublet **16′** (R = 4-tft) is facile with transition state **17′** (R = 4-tft) only 2.9 kcal/mol above **16′** (R = 4-tft). The structure of **17′** (R = 4-tft) is nearly that expected of the "missing" square-pyramidal isomer of **16′** (R = 4-tft) with an axial 4-tft ligand (Figure 14, Cl2−Pt−Cl3 angle = 136.7°).

Spin densities for the R = 4-tft triplets are listed in Table 9. Triplet **2′^{T1}** (R = 4-tft), like **2′^{T1}** (R = Cl), shows large spin density on the Cl atom with the elongated Pt−Cl distance (Cl1). Triplet **2′^{T2}** (R = 4-tft), like **2′^{T2}** (R = Cl), has a more even spin distribution over the Cl atoms with slightly more density on the axial Cl atoms Cl1 and Cl3. Both triplets thus appear to be Cl-to-Pt charge-transfer in character. The spin-density distribution in triplet **2′^{T3}** (R = 4-tft) is quite different. The total Cl spin density is reduced from that in the other triplets with what remains mostly on the axial Cl atoms Cl1 and Cl3. The "missing" spin density is found mostly in the tft ring (0.465 with greatest density at the *ortho* and *para* positions) suggesting significant tft-to-Pt charge-transfer character. The spin-density distribution in optimized square-pyramidal doublet **16′** (R = 4-tft) (Table 9), derived by Cl1 atom removal from

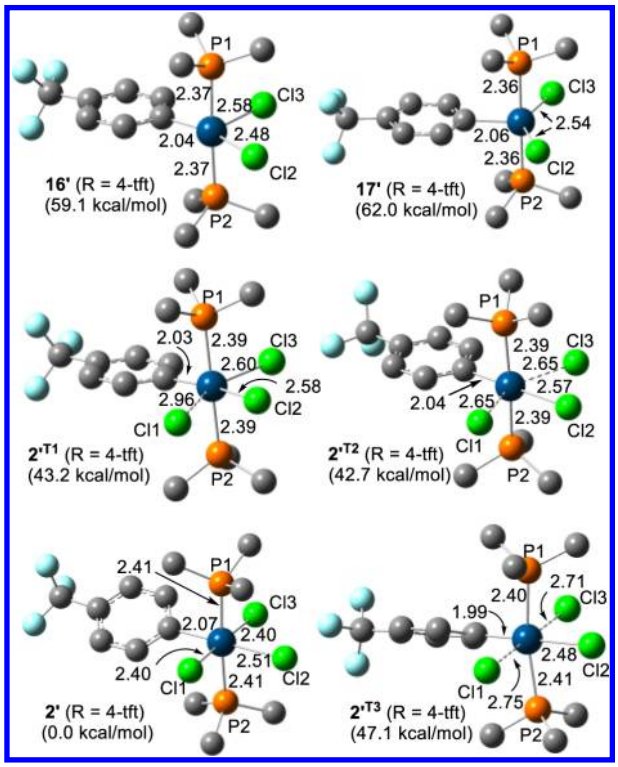

Figure 14. Singlet 2′ (R = 4-tft), triplet **2′^{T1}** (R = 4-tft), **2′^{T2}** (R = 4-tft), **2′^{T3}** (R = 4-tft), doublet **16′** (R = 4-tft), and doublet isomerization transition state **17′** (R = 4-tft) structures from *trans*-Pt(PMe$_3$)$_2$(Cl)$_4$ 2′ (R = 4-tft). Hydrogen atoms omitted. Distances in angstroms, gas-phase energies above singlet 2′ (R = 4-tft) in parentheses (energies for **16′** and **17′** include a Cl radical).

triplet **2′^{T1}** (R = 4-tft), closely resembles that in **16′** (R = Cl) in that the Cl spin density is predominantly located on the axial Cl atom (Cl3).

Relaxed triplet calculations for 2′ (R = phen, 2-tft) were also completed and revealed structures that resemble **2′^{T1}** (R = Cl, 4-tft) in having a unique elongated Pt−Cl bond along the Cl−Pt−Cl axis. However, due to the asymmetry of the R group,

Table 9. Triplet and Doublet Mulliken Atomic Spin Densities (Gas Phase, > 0.01) for R = 4-tft[a]

atom	$2'^{T1}$	$2'^{T2}$	$2'^{T3}$	16′
Pt	0.499	0.495	0.512	0.564
P1	0.016	0.020	0.096	
P2	0.016	0.020	0.092	
Cl1	0.642	0.489	0.352	NA
Cl2	0.488	0.444	0.109	0.050
Cl3	0.289	0.486	0.328	0.306
Cl total	1.419	1.419	0.789	0.356

[a]Spin densities on the $2'^{T3}$ tft ring: C1, 0.153; C2, 0.102; C3, −0.066; C4, 0.213; C5, −0.084; C6, 0.147, C total = 0.465 (atoms numbered sequentially around ring with C1 bonded to Pt).

there are two isomers differing by the side of the R group where the elongated bond is located. Triplets $2'^{T1A}$ (R = phen) and $2'^{T1B}$ (R = phen) are shown in Figure 15 along with the

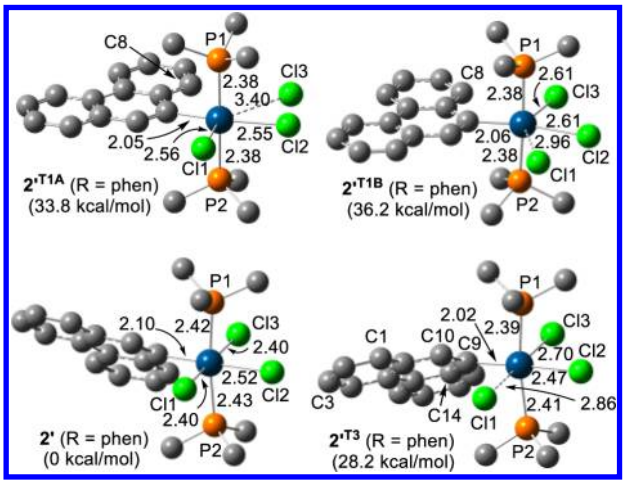

Figure 15. Singlet 2′, triplet $2'^{T1A}$, triplet $2'^{T1A}$, and triplet $2'^{T3}$ (R = phen) structures. Hydrogen atoms omitted. Distances in angstroms, gas-phase energies above singlet 2′ (R = phen) in parentheses.

structure of singlet 2′ (R = phen). Triplet $2'^{T1A}$ has the lowest energy of the two and has the elongated Pt−Cl bond (Pt−Cl1) on the same side as the *peri*-hydrogen atom of the phen group. Triplet $2'^{T1B}$ has the elongated Pt−Cl bond (Pt−Cl3) on the opposite side from the *peri*-hydrogen atom of the phen group. This leaves the more strongly bonded Cl1 in close proximity to the *peri*-hydrogen atom, and this probably accounts for the higher energy of $2'^{T1B}$.

Yet a third triplet structure, $2'^{T3}$ (R = phen), was located for the phen complex. This triplet resembles triplet $2'^{T3}$ (R = 4-tft) in having elongated Pt−Cl distances along the Cl1−Pt−Cl3 axis and other bond distances reduced from the singlet. Unique to $2'^{T3}$ (R = phen) is a distortion of the Pt−phen bonding. In 2′ (R = phen); the Pt atom and the phen ring carbon atoms all lie in a plane, as would be expected. In contrast, $2'^{T3}$ (R = phen) has the Pt atom 0.18 Å and C9 0.83 Å out of the plane formed by all the other phen carbon atoms (largest deviation from plane is 0.06 Å for the other C atoms). Another way of describing the distortion is as a 17° fold of the phen ligand along the C10−C14 vector as measured by the angle between the planes formed by the phen carbon atoms except C9 and the plane formed by Pt, C9, C10, and C14. (See Supporting Information Figure S104 for a drawing of the planes and distances to the planes in $2'^{T3}$ (R = phen).) Examination of

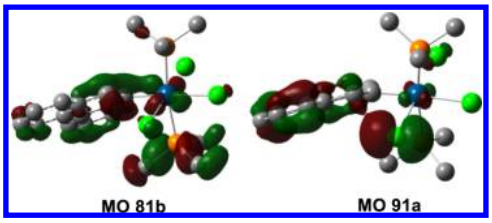

Figure 16. MOs (isovalue = 0.04 e/Å^3, CAM-B3LYP, pcm) for triplet $2'^{T3}$ (R = phen) showing ring-Pt and ring-Cl overlap. Same molecular orientation as in Figure 15 (SOMOs = 98a, 99a).

the upper 16 occupied α and β MOs for $2'^{T3}$ (R = phen) showed only the two orbitals (Figure 16) that might favor the fold. Of particular interest is 91a, which shows a small bonding overlap between chlorine atom Cl1 and phen carbon atom C10. C10 is the ring-chlorination sight in photoproduct **9** (R_{Cl} = Cl-phen). Mulliken spin densities for $2'^{T3}$ (R = phen) are also interesting in this regard and show, with the exception of the Pt center, the largest spin densities on Cl1 and C10 (Table 10). The implication is that this triplet is a model for the

Table 10. Triplet and Doublet[a] Mulliken Atomic Spin Densities (Gas Phase, >0.01) for R = phen

atom	$2'^{T1A}$	$2'^{T1B}$	$2'^{T3}$	$16'^{A}$	$16'^{B}$
Pt	0.607	0.505	0.505	0.608	0.590
P1		0.014	0.024		
P2		0.012	0.024		
Cl1	0.301	0.607	0.353	0.304	NA
Cl2	0.426	0.521	0.024	0.035	0.043
Cl3	0.628	0.300	0.266	NA	0.304
Cl total	1.355	1.428	0.643	0.339	0.347
C total			0.899[b]		

[a]Doublets $16'^{A}$ and $16'^{B}$ are derived by removal of the weakly bonded Cl atoms from $2'^{T1A}$ and $2'^{T1B}$, respectively. [b]Spin densities >0.100 for phen C atoms: C1, 0.121; C3, 0.123; C8, 0.108; C9, 0.247; C10, 0.300. Doublet.

excited-state species involved in the ring-chlorination photochemistry of **2**.

■ DISCUSSION

As shown in Scheme 2 and eq 6 the overall photochemical process for complexes **2** is photoreduction by chlorine elimination. The eliminated chlorine is found in ring chlorination (Table 1), phosphine ligand chlorination (Table 1), alkene chlorination (Scheme 3 and Figure 4), and, most likely, solvent chlorination products. The alkene products clearly indicate that molecular chlorine (Cl_2) is not the chlorinating agent. In particular, the observation of an approximately 50−50 mixture of *syn* and *anti* 2-hexene addition products is not consistent with Cl_2 addition. Chlorination of 2-hexene with Cl_2 gives only the *anti* addition product under similar conditions. The chlorination competition experiment with a mixture of 1-hexene and *trans*-3-hexene further confirms that Cl_2 is not the chlorinating agent in the photochemical reactions and indicates an R group dependent steric factor. With Cl_2 as the chlorinating agent the more electron-rich, but sterically more demanding, *trans*-3-hexene is the favored (by 12:1) chlorination target. Photochlorination with **2** (R = Cl), the least sterically encumbered of the complexes, still favors *trans*-3-hexene, but the bias is much reduced (3:1). With crowded **2** (R = 2-tft) the selection is

inverted (1:3), and the less-electron rich, but sterically less demanding, 1-hexene is the favored chlorination target. This implies that the chlorinating agent is an activated Pt complex which transfers a chlorine atom to the alkene in a step that is susceptible to steric hindrance. The observed mixture of *syn*- and *anti*-addition products is consistent with isomerization of an alkene Cl radical-addition intermediate.

The evident absence of Cl_2 elimination from **2** is in contrast to the analogous bromine systems *trans*-$Pt(PEt_3)_2(R)(Br)_3$ where strong evidence that molecular bromine (Br_2) is the alkene brominating agent was found.[19] However, even in this system, highly reactive alkenes give evidence of radical-like reactivity ascribed to direct reaction of the alkene with a bromo complex excited state. Direct reaction with an excited state is apparently the only alkene reaction pathway for **2**. Interestingly, a similar dichotomy in the aqueous photochemistry of the simple halogen complexes PtX_6^{2-} is observed: The X = Br complex photoeliminates a bromide anion[37] while the X = Cl complex photoeliminates a chlorine radical.[40]

Although we have not probed it in detail, it appears that the photochemistry for **2** (except R = peryl) is essentially the same at 313 and 380 nm (Table 1) suggesting that the complexes follow Kasha's rule[41] that excitation to upper energy levels is followed by rapid internal conversion to the lowest-energy state. Singlet TDDFT calculations indicate that this state is dark for **2** and is found at 521 nm for R = phen in dichloromethane. This value may be underestimated as suggested by the behavior of **2** (R = peryl). Transition energies involving the Pt and Cl ligand orbitals should be similar for the peryl and phen complexes while transitions involving the π systems should be at substantially lower energies for the peryl complex. Excitation at 313 nm into the phen ligand $\pi-\pi^*$ transition of **2** (R = phen) does not give detectable phen ligand fluorescence but does give Pt center reduction indicating internal conversion to the lower energy Pt/Cl-centered excited states. In contrast, excitation into the peryl ligand $\pi-\pi^*$ transition of **2** (R = peryl) at 400 nm gives only peryl-ligand fluorescence. No Pt center photoreduction is observed indicating little to no internal conversion and suggesting that the $\pi-\pi^*$ excited state is at similar or lower energy to the Pt/Cl-centered excited state(s). The photoreduction chemistry of the peryl complex can still be accessed by irradiation into higher energy bands (380 nm), but the quantum yields are low and peryl moiety fluorescence is still observed but at lower quantum yield than with direct excitation into the $\pi-\pi^*$ band. Population of both the $\pi-\pi^*$ and the photoreduction-active excited states from these higher energy states is therefore indicated. Consistent with this interpretation, the analogous bromo complex *trans*-$Pt(PEt_3)_2(peryl)(Br)_3$,[19] which should have lower energy Pt/Br centered excited states (due to the lower energy bromine orbitals), shows strong photoreduction activity with no visible peryl moiety fluorescence even when the peryl $\pi-\pi^*$ band is irradiated at as low an energy as 470 nm.

The 77 K emission wavelengths give a measure of the triplet excited-state energies in **2**. The microsecond lifetimes indicate triplet emission, and assuming that the associated excited states are the lowest-energy triplets, they can be compared to the calculated lowest vertical triplet transitions and the lowest relaxed triplet energies (Table 11). In every case, the emission energy lies between the vertical-transition energy and the relaxed triplet energy. This is to be expected since emission is likely from a vibrationally relaxed triplet to a vibrationally excited singlet. In addition, the rigid matrix should inhibit geometric changes involved in the triplet relaxation giving a strained triplet. Finally, frozen solvents are oriented to the ground state and not the excited state, and this tends to blue-shift emissions.[42] However, the rather small emission energy spread (~2 kcal/mol) over the R groups is notable and in contrast to the much larger spread (15 kcal/mol) in the relaxed-triplet energies.

Table 11. Energy (kcal/mol) Comparison for the Emission, the Lowest-Energy TDDFT Singlet−Triplet Vertical Transitions and Lowest-Energy DFT Relaxed Triplets for 2 or 2′

R	emission	lowest vertical transition	lowest relaxed triplet[a]
4-tft	47.3	64.4	42.7
Cl	48.6	53.2	39.9
2-tft	49.0	63.1	31.7
phen	49.4	55.0	28.2

[a]With respect to the ground-state singlet.

The **2′** triplet excited states revealed in the DFT calculations appear to model the reactive excited states of **2**. High spin density is located on the Cl atoms of the triplets, and Cl radical loss is a facile process indicating that the triplets should be good Cl atom donors. The finding of multiple triplets with close energies indicates that if the lifetimes are sufficient then a triplet equilibrium mixture would be attained. (Multiple triplets are a feature of Ru(II) polypyridyl systems.[43−46]) The R = phen system is a particularly interesting example as triplet $\mathbf{2}'^{T3}$ (R = phen) appears to be a model for a precursor to phen ligand chlorination. Suppression of ring chlorination when reactive substrates are present can then be explained either by reaction of the substrate with $\mathbf{2}'^{T3}$ at a competitive rate to the ring chlorination or by reaction of the substrate with triplets $\mathbf{2}'^{T1A}$ and/or $\mathbf{2}'^{T1B}$ thereby shifting the equilibrium away from $\mathbf{2}'^{T3}$ and slowing the rate of ring chlorination. The latter case is depicted in the proposed Jablonski-type diagram for **2** (R = phen) in Scheme 4 and more generally in the reaction pathway for all **2** in Scheme 5. The role of symmetric triplets $\mathbf{2}'^{T2}$ (R = Cl, 4-tft) in the photochemistry is unclear. The overall spin-density distribution in these triplets is similar to that in $\mathbf{2}'^{T1}$ with the difference that the spin density is the same for each of the Cl atoms and not concentrated on a single Cl atom as in $\mathbf{2}'^{T1}$. This may make $\mathbf{2}'^{T2}$ weaker Cl-atom donors, although, energetically, loss of a Cl atom is no more difficult than for $\mathbf{2}'^{T1}$.

Scheme 4. Proposed Jablonski-type Diagram for 2 (R = phen)[a]

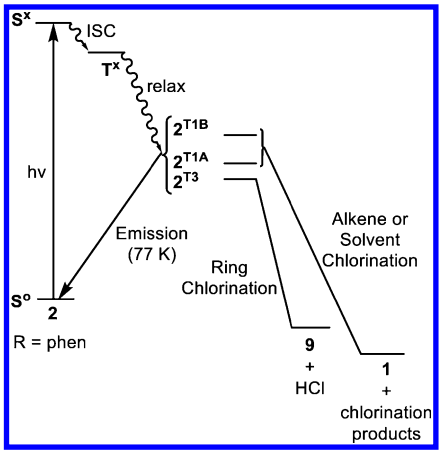

[a]Triplets $\mathbf{2}^{T3}$, $\mathbf{2}^{T1A}$, and/or $\mathbf{2}^{T1B}$ are PEt_3 analogues of model triplets $\mathbf{2}'^{T3}$, $\mathbf{2}'^{T1A}$, and/or $\mathbf{2}'^{T1B}$.

dx.doi.org/10.1021/ic5009413 | Inorg. Chem. XXXX, XXX, XXX−XXX

Scheme 5. Proposed Photoreaction Pathway for 2

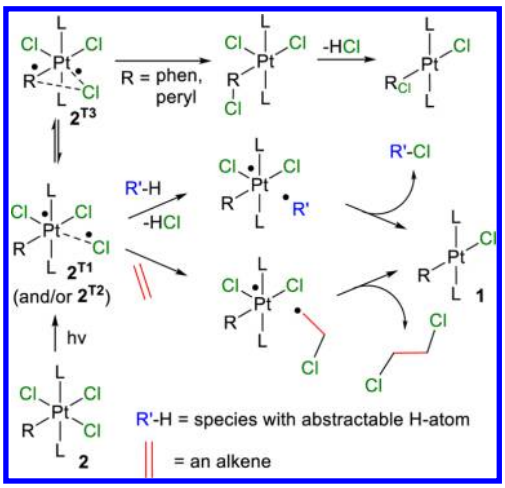

CONCLUSIONS

Solution photoreduction of **2** does not involve molecular chlorine elimination. Instead, the behavior of the system suggests direct reaction of an excited state, or excited states, with added alkenes and/or solvents. DFT modeling and 77 K emission lifetimes indicate that the reactive excited states are triplets with strong Cl-radical donor character. One of these triplets also appears to be responsible for the observed phenanthryl and peryl ligand photochlorination for **2** (R = phen) and **2** (R = peryl). Photoreduction of **2** in the solid state also does not involve any significant amount of molecular chlorine elimination. These results call into question the idea of molecular chlorine photoelimination in other systems where *in situ* alkenes or solvents are used to "trap" putative molecular chlorine.

ASSOCIATED CONTENT

Supporting Information

Experimental details, CIF files, NMR spectra, and DFT data (coordinates, energies, transitions, NTO figures, structures). This material is available free of charge via the Internet at http://pubs.acs.org.

AUTHOR INFORMATION

Corresponding Author

*E-mail: sharpp@missouri.edu.

Author Contributions

The manuscript was written through contributions of all authors. All authors have given approval to the final version of the manuscript.

Notes

The authors declare no competing financial interest.

ACKNOWLEDGMENTS

Support was provided by the U.S. Department of Energy, Office of Basic Energy Sciences (DE-FG02-88ER13880). We thank Dr. Charles Barns for X-ray data collection and processing, Dr. Wei Wycoff for assistance with the NMR measurements, and Alice R. Karikachery for assistance with experimental procedures. The computations were performed on the HPC resources at the University of Missouri Bioinformatics Consortium (UMBC).

REFERENCES

(1) Likhtenshtein, G. *Solar Energy Conversion: Chemical Aspects*; John Wiley & Sons: Hoboken, NJ, 2012.
(2) McKone, J. R.; Lewis, N. S.; Gray, H. B. *Chem. Mater.* **2014**, *24*, 407.
(3) Teets, T. S.; Nocera, D. G. *Chem. Commun.* **2011**, *47*, 9268.
(4) Hagfeldt, A.; Boschloo, G.; Sun, L.; Kloo, L.; Pettersson, H. *Chem. Rev.* **2010**, *110*, 6595.
(5) Nocera, D. G. *Inorg. Chem.* **2009**, *48*, 10001.
(6) Esswein, A. J.; Nocera, D. G. *Chem. Rev.* **2007**, *107*, 4022.
(7) Lewis, N. S.; Nocera, D. G. *Proc. Natl. Acad. Sci. U.S.A.* **2006**, *103*, 15729.
(8) Dempsey, J. L.; Esswein, A. J.; Manke, D. R.; Rosenthal, J.; Soper, J. D.; Nocera, D. G. *Inorg. Chem.* **2005**, *44*, 6879.
(9) Eisenberg, R.; Nocera, D. G. *Inorg. Chem.* **2005**, *44*, 6799.
(10) Kohl, S. W.; Weiner, L.; Schwartsburd, L.; Konstantinovski, L.; Shimon, L. J. W.; Ben-David, Y.; Iron, M. A.; Milstein, D. *Science* **2009**, *324*, 74.
(11) Heyduk, A. F.; Nocera, D. G. *Science* **2001**, *293*, 1639.
(12) Esswein, A. J.; Veige, A. S.; Nocera, D. G. *J. Am. Chem. Soc.* **2005**, *127*, 16641.
(13) Eidem, P. K.; Maverick, A. W.; Gray, H. B. *Inorg. Chim. Acta* **1981**, *50*, 59.
(14) Gray, H. B.; Maverick, A. W. *Science* **1981**, *214*, 1201.
(15) Petruzzella, E.; Margiotta, N.; Ravera, M.; Natile, G. *Inorg. Chem.* **2013**, *52*, 2393.
(16) Lin, T.-P.; Gabbaï, F. P. *J. Am. Chem. Soc.* **2012**, *134*, 12230.
(17) Vogler, A.; Kunkely, H. *Inorg. Chem. Commun.* **2011**, *14*, 96.
(18) Wickramasinghe, L. A.; Sharp, P. R. *Inorg. Chem.* **2014**, *53*, 1430.
(19) Karikachery, A. R.; Lee, H. B.; Masjedi, M.; Ross, A.; Moody, M. A.; Cai, X.; Chui, M.; Hoff, C.; Sharp, P. R. *Inorg. Chem.* **2013**, *52*, 4113.
(20) Cook, T. R.; Surendranath, Y.; Nocera, D. G. *J. Am. Chem. Soc.* **2009**, *131*, 28.
(21) Teets, T. S.; Nocera, D. G. *J. Am. Chem. Soc.* **2009**, *131*, 7411.
(22) Teets, T. S.; Lutterman, D. A.; Nocera, D. G. *Inorg. Chem.* **2010**, *49*, 3035.
(23) Cook, T. R.; McCarthy, B. D.; Lutterman, D. A.; Nocera, D. G. *Inorg. Chem.* **2012**, *51*, 5152.
(24) Lee, C. H.; Lutterman, D. A.; Nocera, D. G. *Dalton Trans.* **2013**, *42*, 2355.
(25) Lentijo, S.; Miguel, J. A.; Espinet, P. *Inorg. Chem.* **2010**, *49*, 9169.
(26) Parshall, G. W. *Inorg. Synth.* **1970**, *12*, 26.
(27) Nakamura, Y.; Tsuihiji, T.; Mita, T.; Minowa, T.; Tobita, S.; Shizuka, H.; Nishimura, J. *J. Am. Chem. Soc.* **1996**, *118*, 1006.
(28) Hu, J.; Yip, J. H. K.; Ma, D.-L.; Wong, K.-Y.; Chung, W.-H. *Organometallics* **2008**, *28*, 51.
(29) Taft, R. W. *J. Am. Chem. Soc.* **1948**, *70*, 3364.
(30) McCall, A. S.; Wang, H.; Desper, J. M.; Kraft, S. *J. Am. Chem. Soc.* **2011**, *133*, 1832.
(31) Logan, S. R. *Fundamentals of Chemical Kinetics*; Longman: Harlow, U.K., 1996.
(32) Perez-Benito, J. F.; Arias, C.; Brillas, E. *An. Quim.* **1991**, *87*, 849.
(33) Anderson, D. W. W.; Ebsworth, E. A. V.; Rankin, D. W. H. *J. Chem. Soc., Dalton Trans.* **1973**, 854.
(34) Bazhin, N. M.; Gritsan, N. P.; Korolev, V. V.; Camyshan, S. V. *J. Lumin.* **1987**, *37*, 87.
(35) Martin, R. L.; Hay, P. J.; Pratt, L. R. *J. Phys. Chem. A* **1998**, *102*, 3565.
(36) Sieffert, N.; Bühl, M. *J. Am. Chem. Soc.* **2010**, *132*, 8056.
(37) Zheldakov, I. L.; N. Ryazantsev, M.; Tarnovsky, A. N. *J. Phys. Chem. Lett.* **2011**, *2*, 1540.
(38) Ruiz, E.; Cirera, J.; Alvarez, S. *Coord. Chem. Rev.* **2005**, *249*, 2649.
(39) Luo, Y.-R. *Comprehensive Handbook of Chemical Bond Energies*; CRC Press: Boca Raton, FL, 2007.

(40) Glebov, E. M.; Kolomeets, A. V.; Pozdnyakov, I. P.; Plyusnin, V. F.; Grivin, V. P.; Tkachenko, N. V.; Lemmetyinen, H. *RSC Adv.* **2012**, *2*, 5768 and references cited therein.
(41) Kasha, M. *Discuss. Faraday Soc.* **1950**, *9*, 14.
(42) Tamayo, A. B.; Garon, S.; Sajoto, T.; Djurovich, P. I.; Tsyba, I. M.; Bau, R.; Thompson, M. E. *Inorg. Chem.* **2005**, *44*, 8723.
(43) Alary, F.; Heully, J. L.; Bijeire, L.; Vicendo, P. *Inorg. Chem.* **2007**, *46*, 3154.
(44) Österman, T.; Abrahamsson, M.; Becker, H.-C.; Hammarström, L.; Persson, P. *J. Phys. Chem. A* **2011**, *116*, 1041.
(45) Salassa, L.; Garino, C.; Salassa, G.; Gobetto, R.; Nervi, C. *J. Am. Chem. Soc.* **2008**, *130*, 9590.
(46) Borfecchia, E.; Garino, C.; Salassa, L.; Ruiu, T.; Gianolio, D.; Zhang, X.; Attenkofer, K.; Chen, L. X.; Gobetto, R.; Sadler, P. J.; Lamberti, C. *Dalton Trans.* **2013**, *42*, 6564.